




High Power Conversion Efficiency Narrow Divergence Angle Photonic Crystal Laser Diodes

Liang Wang , Aiyi Qi, Xuyan Zhou , Ting Fu , Chuanwang Xu, Renbo Han, Hongwei Qu, and Wanhua Zheng 

Abstract—9xx nm laser diodes (LDs) with aluminum component continuous gradient photonic band crystal (CCG-PBC) waveguide structure are designed and fabricated. The simulation results indicate that the CCG-PBC structure can significantly reduce the heterojunction barrier and carrier accumulation at the interface of the conventional PBC structure. We demonstrate that the LD with CCG-PBC structure can achieve a narrow vertical divergence angle of 16.2° at full width at half maximum, and the divergence angle changes with current not more than 0.5° . Meanwhile, the power conversion efficiency (PCE) of the narrow divergence angle LD can reach 66.7%, and the PCE at 20 W is still over 60%. After optimizing the coating reflectivity and cavity length of the CCG-PBC structure LD, the peak PCE and power are 71.5% and 17.2 W at 25°C and 77.7% and 23.3 W at 0°C , respectively, which are optimal results for any edge-emitting LD. Our device provides valuable guidance for researching high power and high efficiency narrow vertical divergence angle LDs.

Index Terms—High efficiency, photonic crystal, laser diodes, narrow divergence.

I. INTRODUCTION

9xx nm high-power laser diodes are increasingly being used directly in material processing applications due to their low cost and high efficiency [1]. Nevertheless, they are more often used as efficient pump sources for other solid state gain media [2]–[5], such as fiber lasers [6] and erbium-doped fiber amplifiers (EDFA) [7]. In these applications, LDs usually need to be coupled with optical fibers [7], or volume Bragg gratings [8] to form a module. Therefore, to satisfy the requirement of module efficiency in the industry, it is necessary to improve not only the power conversion efficiency (PCE) of LDs but also the coupling efficiency of lasers and fibers. 9xx nm edge-emitting LDs can currently achieve peak PCEs of more than 70% [9], [10], however, their large vertical divergence angle ($\sim 40^\circ$) [11], making low coupling efficiency with optical components and tight alignment tolerances, limit their applications. Several approaches have been introduced in laser designs to reduce the vertical divergence angle, such as the super large optical cavity (SLOC) [12] and the photonic band crystal (PBC) waveguide [13]–[15]. Both SLOC and PBC designs demonstrated vertical divergence angle less than 11° at full width at half maximum (FWHM), but their continuous wave (CW) output powers did not exceed 10 W and the PCEs were less than 60% [11], [12], [14], [15]. In reference [16], we have achieved a maximum output power of 18.8 W and a peak PCE of 62% by optimizing the structure of the PBC waveguide and the position of the quantum well (QW), while maintaining a narrow vertical divergence angle of 16° (FWHM) [16]. However, the 62% PCE is still far from the 70% PCE of conventional edge-emitting LDs.

We designed a component continuous gradient PBC (CCG-PBC) waveguide structure to help LD get with both high efficiency and narrow vertical divergence angle. Firstly, we simulated and compared the CCG-PBC structure with the conventional PBC structure, by the commercial software LaserMod [12]. By calculating the effects of different parameters on the external differential quantum efficiency, the CCG-PBC epitaxial structures were designed and the LDs were fabricated. Finally, the electro-optical properties of LDs with CCG-PBC structure were investigated. The measured results were consistent with the simulated results.

Manuscript received 26 May 2022; revised 10 July 2022; accepted 18 July 2022. Date of publication 21 July 2022; date of current version 9 August 2022. This work was supported in part by the National Natural Science Foundation of China under Grant 91850206, and in part by the Major Scientific Research Instrument Development Project of Chinese Academy of Sciences under Grant ZDKYYQ20220003. (Liang Wang and Aiyi Qi contributed equally to this work.) (Corresponding authors: Xuyan Zhou; Wanhua Zheng.)

Liang Wang and Renbo Han are with the Key Laboratory of Solid-State Optoelectronics Information Technology, Institute of Semiconductors, Chinese Academy of Sciences, Beijing 100083, China, and also with the College of Future Technology, University of Chinese Academy of Sciences, Beijing 100049, China (e-mail: wangliang@semi.ac.cn; hanrenbo@semi.ac.cn).

Aiyi Qi and Hongwei Qu are with the Key Laboratory of Solid-State Optoelectronics Information Technology, Institute of Semiconductors, Chinese Academy of Sciences, Beijing 100083, China, with the State Key Laboratory on Integrated Optoelectronics, Institute of Semiconductors, Chinese Academy of Sciences, Beijing 100083, China, and also with the Weifang Academy of Advanced Opto-Electronic Circuits, Weifang 261021, China (e-mail: qiaiyi@semi.ac.cn; quhw@semi.ac.cn).

Xuyan Zhou is with the Key Laboratory of Solid-State Optoelectronics Information Technology, Institute of Semiconductors, Chinese Academy of Sciences, Beijing 100083, China, and also with the Weifang Academy of Advanced Opto-Electronic Circuits, Weifang 261021, China (e-mail: zhouxuyan@semi.ac.cn).

Ting Fu and Chuanwang Xu are with the Key Laboratory of Solid-State Optoelectronics Information Technology, Institute of Semiconductors, Chinese Academy of Sciences, Beijing 100083, China, and also with the Center of Materials Science and Optoelectronics Engineering, University of Chinese Academy of Sciences, Beijing 101408, China (e-mail: futing@semi.ac.cn; xuchuanwang@semi.ac.cn).

Wanhua Zheng is with the Key Laboratory of Solid-State Optoelectronics Information Technology, Institute of Semiconductors, Chinese Academy of Sciences, Beijing 100083, China, with the State Key Laboratory on Integrated Optoelectronics, Institute of Semiconductors, Chinese Academy of Sciences, Beijing 100083, China, with the Center of Materials Science and Optoelectronics Engineering, University of Chinese Academy of Sciences, Beijing 101408, China, with the College of Future Technology, University of Chinese Academy of Sciences, Beijing 100049, China, and also with the Weifang Academy of Advanced Opto-Electronic Circuits, Weifang 261021, China (e-mail: whzheng@semi.ac.cn).

Digital Object Identifier 10.1109/JPHOT.2022.3192929

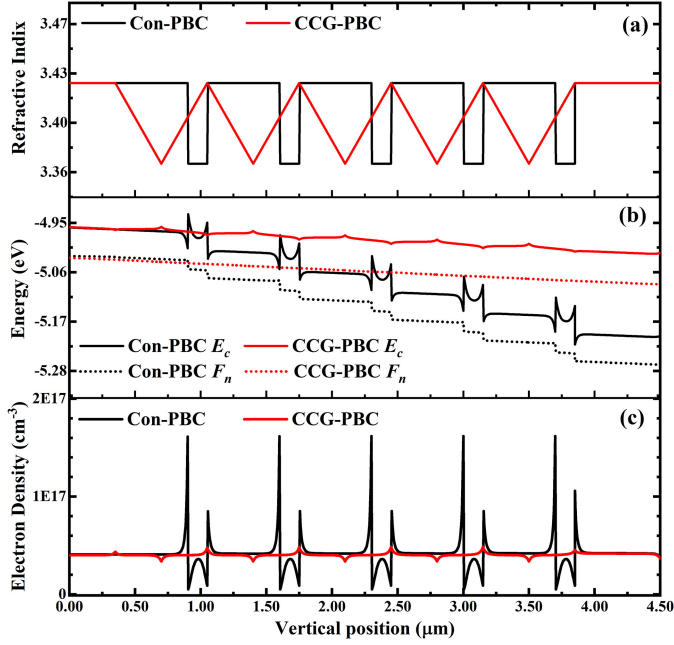


Fig. 1. (a) Refractive index distribution of the Con-PBC structure and CCG-PBC structure. (b) Energy band distribution (E_c (solid line) is the conduction band, F_n (dotted line) is the electron quasi-Fermi energy level) simulated at 20 A. (c) Electron density distribution of the Con-PBC structure (black line) and CCG-PBC structure (red line) simulated at 20 A.

II. CALCULATIONS AND SIMULATIONS

At present, longitudinal structures with narrow vertical divergence angle are mostly achieved by SLOC and PBC designs. Compared with the SLOC design, the PBC design has a thinner epitaxial thickness, and the vertical divergence angle is not sensitive to the change of current. Therefore, the LD with a PBC design could have higher power, higher efficiency, and narrower vertical divergence angle at the same time. However, the conventional PBC (Con-PBC) structure is made by alternating refractive index layers [11], [13]–[17], as shown in Fig. 1(a), which introduces additional heterogeneous interfaces. The discontinuity of the energy band at the heterogeneous interfaces causes interfacial barriers, as shown in Fig. 1(b). These barriers lead to carrier accumulation at the interface, as shown in Fig. 1(c), which results in the higher operating voltage of the LD, as shown in Fig. 2, and causes additional carrier loss and optical loss. Therefore, we designed a PBC structure, called aluminum component continuous gradient PBC (CCG-PBC) structure, to eliminate the potential barrier and carrier accumulation at the heterogeneous interface, as shown in Fig. 1.

The CCG-PBC structure can greatly improve the internal quantum efficiency η_i of the LD, meanwhile, reducing the absorption loss in the waveguide $\alpha_{i,WG}$ and the operating voltage V of the LD, and increase the optical output power P_{out} and the PCE consequently. The P_{out} and the PCE of LD can be expressed as

$$P_{out} = \eta_d \frac{h\nu}{q} (I - I_{th}) \quad (1)$$

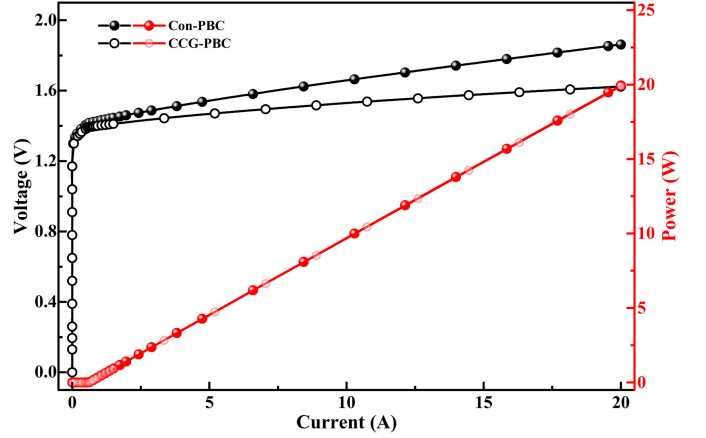


Fig. 2. Power–Voltage–Current curves of the Con-PBC and CCG-PBC structure LDs simulated at 300K.

$$PCE = \frac{P_{out}}{IV} = \eta_d \frac{h\nu}{q} \times \frac{I - I_{th}}{I(V_0 + IR_s)}. \quad (2)$$

Here $h\nu$ is the photon energy, q is the elementary charge, η_d is the external differential quantum efficiency, I_{th} is the threshold current, V_0 is the turn-on voltage and R_s is the series resistance of the LD. Therefore, the increase of η_d and the decrease of R_s are very beneficial to improve the P_{out} and PCE of LD at large injection currents. The external differential quantum efficiency η_d is proportional to the internal quantum efficiency η_i :

$$\eta_d = \eta_i \frac{\alpha_m}{\alpha_i + \alpha_m}. \quad (3)$$

Here α_m is mirror loss and α_i represents internal loss. α_m is related with the cavity length L , front-facet reflectivity R_f and back-facet reflectivity R_b :

$$\alpha_m = \frac{1}{2L} \ln \frac{1}{R_f R_b}. \quad (4)$$

And the internal loss is approximated as the sum of free carrier absorption (FCA) loss from the waveguide and the quantum well [18]

$$\alpha_i \approx \alpha_{i,WG}^{(FCA)} + \alpha_{i,QW}^{(FCA)}. \quad (5)$$

FCA loss in the waveguide is calculated by

$$\alpha_{i,WG}^{(FCA)} \approx \Gamma_p \sigma_p N_p + \Gamma_n \sigma_n N_n, \quad (6)$$

and FCA loss in the quantum well is calculated by

$$\alpha_{i,QW}^{(FCA)} \approx \Gamma N_{th} (\sigma_n + \sigma_p). \quad (7)$$

Here Γ_p , Γ_n and Γ are the optical confinement factor for the p waveguide, n waveguide and quantum well. The fundamental mode is almost entirely restricted to the three layers, so the optical confinement factors should satisfy the relation, $\Gamma_p + \Gamma_n + \Gamma \approx 1$. σ_p and σ_n are the absorption cross sections for holes and electrons, respectively. N_p and N_n are the free-carrier densities (roughly the doping level for CCG-PBC structure) of electrons and holes in the waveguide layer, and N_{th} is the threshold carrier

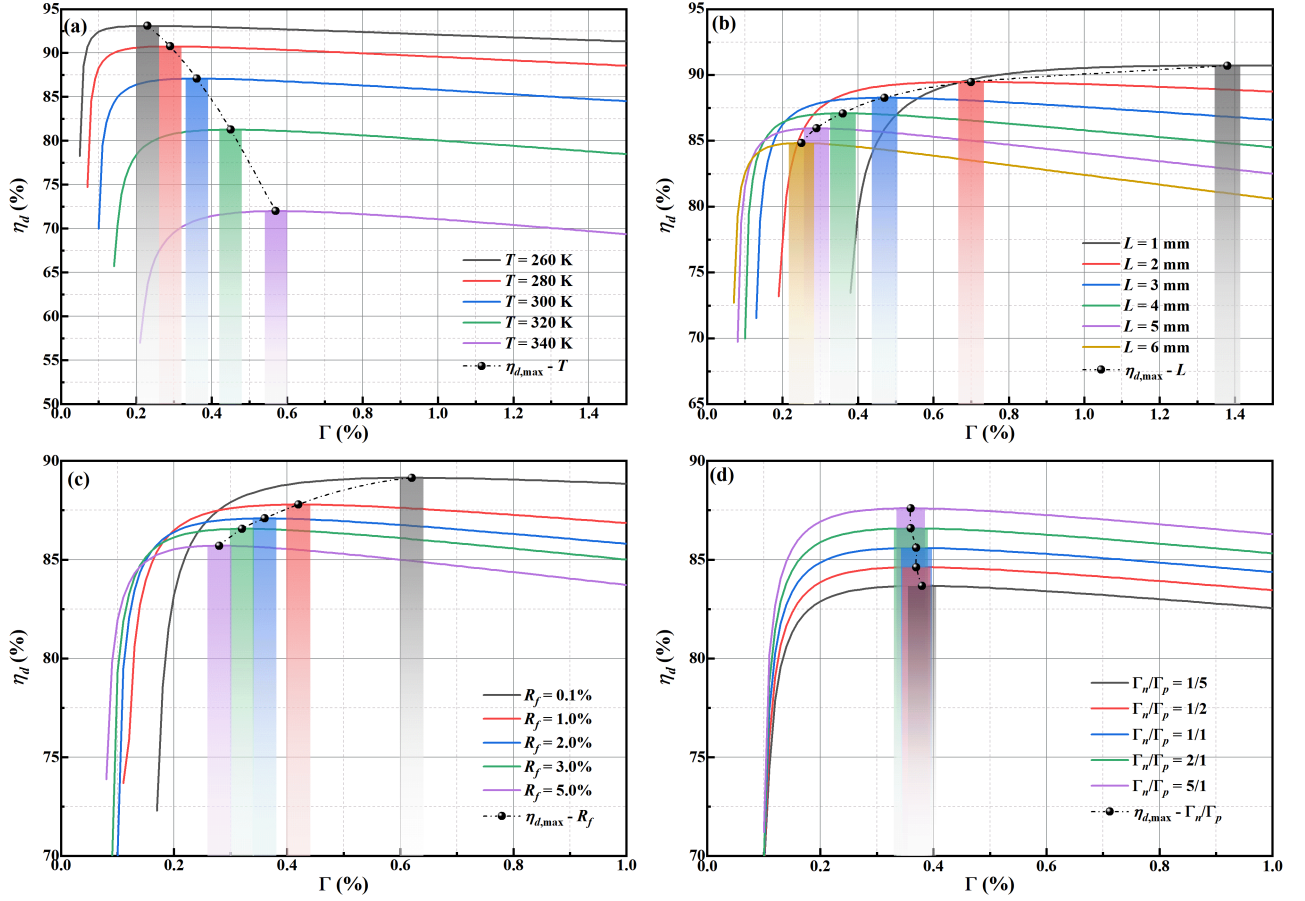


Fig. 3. The variation of η_d with Γ for (a) different T , (b) different L , (c) different R_f , and (d) different Γ_n/Γ_p . The balls and bars denote the maximum value of η_d and the corresponding Γ value for each condition, respectively.

density in the quantum well. N_{th} can be calculated by

$$N_{th} = N_{tr} \exp\left(\frac{\alpha_i + \alpha_m}{\Gamma g_0}\right). \quad (8)$$

Here, N_{tr} is the transparency carrier density, and g_0 is the differential gain. If the influence of temperature is considered, only σ_p , σ_n , η_i , N_{tr} , and g_0 are affected by temperature in (3)–(8), which can be expressed as [18]–[20]

$$\sigma_n(T) = \sigma_{n,0} \frac{T}{300K}, \quad \sigma_p(T) = \sigma_{p,0} \left(\frac{T}{300K}\right)^2, \quad (9)$$

$$\eta_i(T) = 1 - \eta_{i,0} \exp\left(\frac{T - 300K}{T_i}\right), \quad (10)$$

$$N_{tr}(T) = N_{tr,0} \exp\left(\frac{T - 300K}{T_a}\right), \quad (11)$$

$$g_0(T) = g_{0,0} \exp\left(-\frac{T - 300K}{T_a}\right). \quad (12)$$

Here $\sigma_{n,0}$, $\sigma_{p,0}$, $\eta_{i,0}$, $N_{tr,0}$ and $g_{0,0}$ are the values at 300 K [18], [20], [21]. T_i and T_a are defined as the characteristic temperature for $1 - \eta_i$ and the active region, respectively [19], [21]. T is the temperature of the active region. Therefore, associating (3)–(12), we can calculate the effect of different parameters on

η_d , the calculation results are shown in Fig. 3, and the parameters involved in the calculation process adopt the typical values of the 9xx nm LD, as shown in Table I.

Fig. 3 shows the variation of η_d with Γ . As Γ increases, η_d grows rapidly to a maximum value $\eta_{d,max}$ and then decreases slowly. As shown in Fig. 3(a), $\eta_{d,max}$ decreases rapidly as the temperature rises, and the corresponding Γ increases at an increasing rate, which means that the higher Γ is more suitable for operation at high temperatures. The temperature of the active area is about 340 K for a 20 W LD at room temperature, so to maximize efficiency at this power, the optimal value of Γ is about 0.6%. From Fig. 3(b), we can see that as L increases, $\eta_{d,max}$ becomes smaller, and the corresponding Γ decreases at a smaller and smaller rate, indicating that the higher Γ is more suitable for making short cavity devices, and the lower Γ corresponds to the longer optimal L . Similarly, it can be concluded from Fig. 3(c) that the smaller the R_f , the larger the η_d at high Γ values. For a low Γ value, it is not that the smaller the R_f , the larger the η_d , but that there exists an optimal R_f . In Fig. 3(d), it can be seen that with the increase of Γ_n/Γ_p , $\eta_{d,max}$ becomes larger uniformly, and the corresponding Γ is almost unchanged. In other words, the larger the Γ_n/Γ_p , the larger the η_d . However, in the design process, when Γ_p becomes smaller, Γ may also become smaller. A too-small Γ will compensate for the benefits of the larger

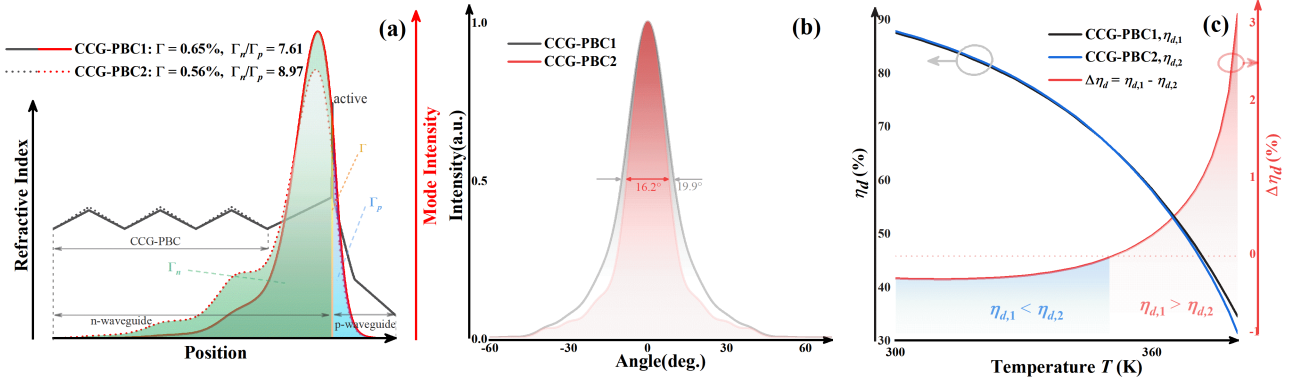


Fig. 4. (a) Refractive index and mode distributions in CCG-PBC1 and CCG-PBC2 waveguide structure. (b) Calculated vertical divergence angles of CCG-PBC1 and CCG-PBC2 waveguide structure. (c) Variation of η_d and difference $\Delta\eta_d$ with T for CCG-PBC1 and CCG-PBC2 structures.

TABLE I
PARAMETERS FOR 9XX nm SINGLE QW LD CALCULATION

Parameters	Value	Units
$\sigma_{n,0}$	3.7×10^{-18}	cm^2
$\sigma_{p,0}$	11×10^{-18}	cm^2
$\eta_{i,0}$	0.05	1
$N_{tr,0}$	1.2×10^{18}	cm^{-3}
$g_{0,0}$	1500	cm^{-1}
T_i	35	K
T_a	100	K
Γ_n/Γ_p	3	1
L	0.4	cm
N_n	5×10^{16}	cm^{-3}
N_p	5×10^{16}	cm^{-3}
R_f	0.02	1
R_b	0.98	1
T	300	K

Γ_n/Γ_p . Therefore, when designing the longitudinal CCG-PBC epitaxial structure, the optimal Γ can be chosen to maximize η_d according to different working conditions. Increasing Γ_n/Γ_p as much as possible while keeping Γ constant can further increase η_d .

III. DESIGN AND FABRICATION

According to the above discussion, the CCG-PBC structure is introduced based on the epitaxial structure of reference [22], and the aluminum composition and thickness of each layer are carefully designed. By adjusting the refractive index in the CCG-PBC structure, which can change the PBC penetration of the fundamental mode, we designed two epitaxial structures with $\Gamma = 0.65\%$ and 0.56% , and $\Gamma_n/\Gamma_p = 7.61$ and 8.97 , respectively. The refractive index and mode distributions of the two CCG-PBC waveguide structures are shown in Fig. 4(a).

Fig. 4(b) shows their calculated vertical divergence angles of 19.9° and 16.2° , respectively. The structure with stronger PBC penetration of fundamental mode, has a narrower divergence angle and a larger Γ_n/Γ_p , but a smaller Γ . The variation of η_d and differences $\Delta\eta_d$ with T are calculated by bringing their Γ and Γ_n/Γ_p into (3)–(12), as shown in Fig. 4(c). It can be seen that η_d decreases more and more rapidly with increasing T . At low T (< 350 K), the η_d of the low- Γ structure CCG-PBC2 is larger than that of the high- Γ structure CCG-PBC1, and the difference between them is almost constant. However, at high T , the η_d of CCG-PBC1 will be larger than that of CCG-PBC2, and the difference between them becomes exponentially larger with increasing T . During device operation, T is proportional to the dissipated power P_{diss} and the slope efficiency S is proportional to η_d , which can be expressed as

$$T = T_{hs} + R_{th}P_{diss} = T_{hs} + R_{th}(IV - P_{out}), \quad (13)$$

$$S = \frac{hv}{q}\eta_d, \quad (14)$$

where R_{th} is the thermal resistance and T_{hs} is the heatsink temperature. Therefore, we may conclude that as the injection current increases, T rises gradually. When T is higher than a certain degree, S becomes very small and the device appears thermal power saturation. Besides, the structure with low- Γ is more likely to saturate. In other words, CCG-PBC1 structure is more likely to have higher power and efficiency than CCG-PBC2 structure at high currents.

Two CCG-PBC structures are grown on GaAs substrates by metal organic chemical vapor deposition. The doping distribution is carefully optimized to lower the resistance, while the loss almost keeps constant. The measured internal losses of the CCG-PBC1 and CCG-PBC2 structures at 25°C are 0.58 cm^{-1} and 0.63 cm^{-1} , respectively. Then, the wafers are processed into broad area (BA) LDs with a stripe width W of $200 \mu\text{m}$ and a cavity length L of 4 mm . The fabrication process includes photolithography, wet etching, SiO_2 dielectric layer growth, p-side Ti/Pt/Au electrode growth, wafer thinning (remaining thickness $< 150 \mu\text{m}$), and n-side AuGeNi/Au electrode growth, etc. After coating the front-facet with 2% anti-reflective and the back-facet with 98% high-reflective, the BA LDs are mounted p-side down

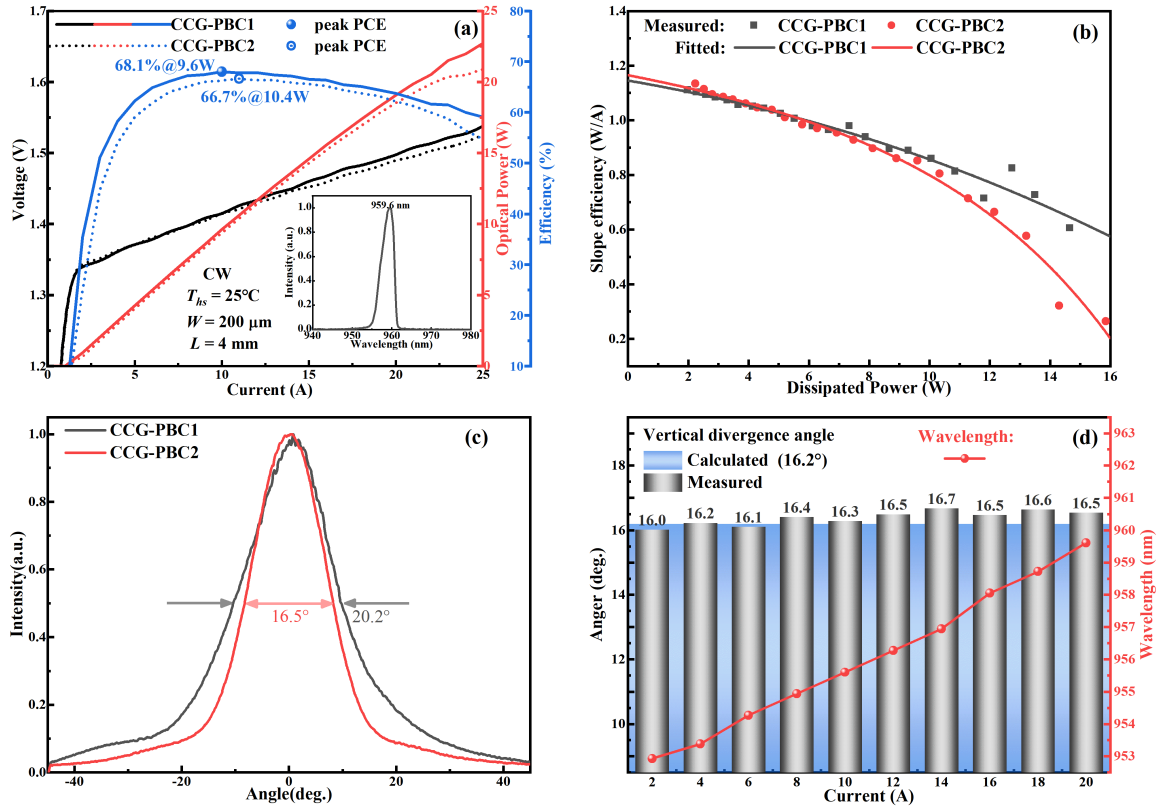


Fig. 5. (a) Voltage, optical power and conversion efficiency versus current for a CCG-PBC1 (solid line) and a CCG-PBC2 (dashed line) structure LD, tested in CW mode at 25°C . The inset shows the emission wavelength of the LD at 20 A. (b) Slope efficiency versus dissipated power for CCG-PBC1 and CCG-PBC2 structure LD. The dots are measured and the lines are fitted. (c) Measured vertical divergence angles of CCG-PBC1 and CCG-PBC2 structure LD at 20 A. (d) The vertical divergence angle (left axis) and emission wavelength (right axis) versus current for the CCG-PBC2 structure LD.

on an aluminum nitride heat sink. At last, their electro-optical performances are measured directly by RB-CT1000 series COS comprehensive performance tester from Shenzhen RAYBOW OPTO.

IV. RESULTS AND DISCUSSIONS

Fig. 5 shows the electro-optical performance measurement results for the CCG-PBC1 and CCG-PBC2 structure LDs in CW mode at 25°C . In Fig. 5(a), the peak PCE of CCG-PBC1 is 68.1% and the peak PCE of CCG-PBC2 is 66.7%, and the PCE exceeds 60% for both structures at 20 W. The results are similar for CCG-PBC1 and CCG-PBC2 with R_s of 8.5 m Ω and 7.8 m Ω , I_{th} of 1.1 A and 1.4 A, and power of 19.1 W and 18.5 W at 20 A, respectively. However, S of CCG-PBC2 decreases more rapidly with the increase of P_{diss} , as shown in Fig. 5(b), so the power of CCG-PBC2 shows significant thermal saturation at currents greater than 20 A, which is consistent with the simulation results in Fig. 4(c). The vertical divergence angles of CCG-PBC1 and CCG-PBC2 at 20 A are 20.2° and 16.5°, respectively, as shown in Fig. 5(c), which are comparable to the calculated results in Fig. 4(b). Fig. 5(d) presents the divergence angles and emission wavelengths of CCG-PBC2 at different currents. The difference between the measured and calculated results of the divergence angles does not exceed 0.5°, which exhibits excellent current insensitivity of the CGC-PBC structure. And the R_{th} calculated from the wavelength change is 2.5 K/W.

From the calculation results in Fig. 3, it is known that for a structure with a determined Γ , there exists an optimal L and R_f to make η_d optimal, which means that the efficiency of the device can be further improved by carefully optimizing L and R_f . The LD with a cavity length of 3.6 mm, a stripe width of 100 μm , and $R_f = 0.6\%$ is fabricated with the epitaxial structure of CCG-PBC1 by calculation, and its electro-optical characteristics are measured at different T_{hs} , as shown in Fig. 6(a). The η_d of the optimized LD is relatively improved by 3.8%, and the peak PCE can reach 71.5% at 25°C and 77.7% at 0°C , which is comparable to or even better than that of a classical edge-emitting LD. However, due to the smaller L and W , the heat dissipation area becomes smaller, so the temperature rise in the active region becomes faster, and the power at 25°C reaches saturation at only 17.2 W. When the T_{hs} is lowered to 0°C , the LD power can reach a maximum of 23.3 W. This indicates that the CCG-PBC1 structure has poor thermal characteristics and is not suitable for operation at high active region temperatures. In other words, the CCG-PBC1 structure is more suitable for low-power high-efficiency devices, high-power high-efficiency devices with long cavities and wide surfaces, or devices that operate at low temperatures. As shown in Fig. 6(b), $L = 3.6 \text{ mm}$ devices at $T_{hs} = 25^\circ\text{C}$ can achieve high efficiency operation with PCE > 70% at $P < 10 \text{ W}$. Besides, $L = 4 \text{ mm}$ devices and $L = 3.6 \text{ mm}$ devices at $T_{hs} = 0^\circ\text{C}$ still maintain their PCE above 60% at $P > 20 \text{ W}$. Therefore, the saturation power of CCG-PBC structured LDs needs to be further improved in future work.

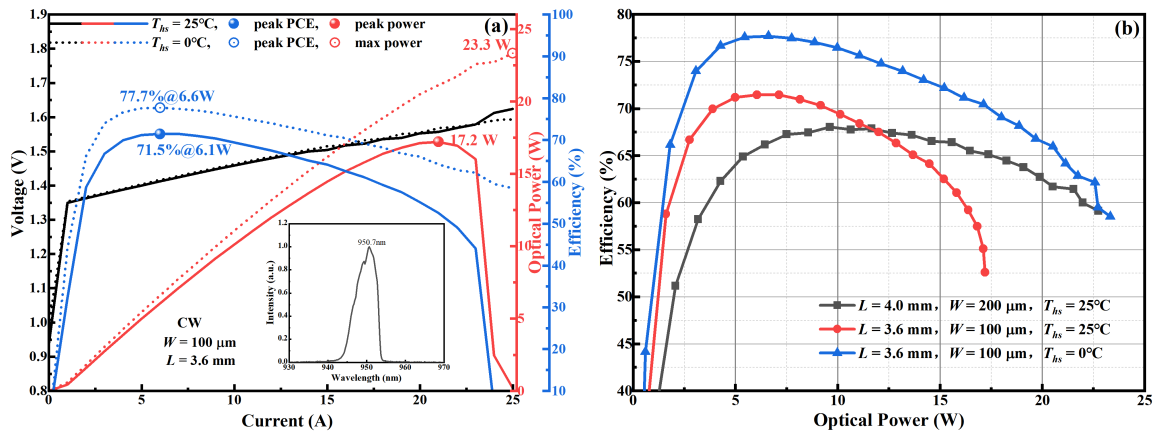


Fig. 6. Voltage, optical power and conversion efficiency versus current for a CCG-PBC1 structure LD, tested in CW mode at 25°C (solid line) and 0°C (dotted line). The inset shows the emission wavelength of the LD at $T_{hs} = 0^\circ\text{C}$ and $I = 25 \text{ A}$. (b) The conversion efficiency versus power for different cavity length and stripe width devices at different heatsink temperatures.

V. CONCLUSION

In summary, we propose an aluminum CCG-PBC waveguide structure to achieve high power and high efficiency operation for narrow vertical divergence angle LD. The LD of the CCG-PBC structure has narrow divergence angle characteristics, when keeping the efficiency and power comparable to the classical edge-emitting LD. The peak efficiency of our CCG-PBC structure LD can reach 71.5% in CW mode. In addition, the measured vertical divergence angle is consistent with the simulation results, and the change of the divergence angle with current does not exceed 0.5° . At the heatsink temperature of 0°C , the peak efficiency can reach 77.7%, and the power can reach 23.3 W, which is a pretty high value for any edge-emitting LD.

REFERENCES

- [1] S. Strohmaier, H. An, and T. Vethake, "Industrial high-power diode lasers: Reliability, power, and brightness," in *Proc. High-Power Diode Laser Technol. Appl. X*, San Francisco, CA, USA, Feb. 2012, vol. 8241, pp. 267–271, doi: [10.1117/12.906832](https://doi.org/10.1117/12.906832).
- [2] B. Köhler et al., "Scalable high-power and high-brightness fiber coupled diode laser devices," in *Proc. High-Power Diode Laser Technol. Appl. X*, San Francisco, CA, USA, Feb. 2012, pp. 36–44, doi: [10.1117/12.909189](https://doi.org/10.1117/12.909189).
- [3] A. Langner et al., "Multi-kW single fiber laser based on an extra large mode area fiber design," in *Proc. Fiber Lasers IX: Technol., Syst., Appl.*, San Francisco, CA, USA, Feb. 2012, pp. 42–53, doi: [10.1117/12.904951](https://doi.org/10.1117/12.904951).
- [4] H. Yu et al., "1.2-kW single-mode fiber laser based on 100-W high-brightness pump diodes," in *Proc. Fiber Lasers IX: Technol., Syst., Appl.*, San Francisco, CA, USA, Feb. 2012, pp. 54–60, doi: [10.1117/12.908454](https://doi.org/10.1117/12.908454).
- [5] J. Malchus, V. Krause, A. Koesters, and D. G. Matthews, "A 25kW fiber-coupled diode laser for pumping applications," in *Proc. High-Power Diode Laser Technol. Appl. XII*, San Francisco, CA, USA, Mar. 2014, pp. 62–71, doi: [10.1117/12.2039110](https://doi.org/10.1117/12.2039110).
- [6] M. Levy et al., "Development of asymmetric epitaxial structures for 65% efficiency laser diodes in the 9xx-nm range," in *Proc. High-Power Diode Laser Technol. Appl. VIII*, San Francisco, CA, USA, Feb. 2010, pp. 179–186, doi: [10.1117/12.843661](https://doi.org/10.1117/12.843661).
- [7] B. Sverdlov et al., "Optimization of fiber coupling in ultra-high power pump modules at $\lambda = 980 \text{ nm}$," in *Proc. High-Power Diode Laser Technol. Appl. XI*, San Francisco, CA, USA, Feb. 2013, pp. 45–54, doi: [10.1117/12.2003999](https://doi.org/10.1117/12.2003999).
- [8] P. Crump et al., "Low-loss smile-insensitive external frequency-stabilization of high power diode lasers enabled by vertical designs with extremely low divergence angle and high efficiency," in *Proc. High-Power Diode Laser Technol. Appl. XI*, San Francisco, CA, USA, Feb. 2013, pp. 208–220, doi: [10.1117/12.2000528](https://doi.org/10.1117/12.2000528).
- [9] Y. Yamagata, Y. Kaifuchi, R. Nogawa, K. Yoshida, R. Morohashi, and M. Yamaguchi, "Highly efficient 9xx-nm band single emitter laser diodes optimized for high output power operation," in *Proc. High-Power Diode Laser Technol. XVIII*, San Francisco, CA, USA, Mar. 2020, pp. 10–15, doi: [10.1117/12.2545721](https://doi.org/10.1117/12.2545721).
- [10] K. Jiang et al., "76% maximum wall plug efficiency of 940 nm laser diode with step graded index structure," *Chin. J. Laser*, vol. 41, no. 4, 2014, Art. no. 0402003, doi: [10.3788/CJL201441.0402003](https://doi.org/10.3788/CJL201441.0402003).
- [11] L. Liu et al., "High-power narrow-vertical-divergence photonic band crystal laser diodes with optimized epitaxial structure," *Appl. Phys. Lett.*, vol. 105, no. 23, Dec. 2014, Art. no. 231110, doi: [10.1063/1.4903883](https://doi.org/10.1063/1.4903883).
- [12] S. Zhao et al., "High-power high-brightness 980 nm lasers with >50% wall-plug efficiency based on asymmetric super large optical cavity," *Opt. Exp.*, vol. 26, no. 3, pp. 3518–3526, Feb. 2018, doi: [10.1364/OE.26.003518](https://doi.org/10.1364/OE.26.003518).
- [13] N. N. Ledentsov and V. A. Shchukin, "Novel concepts for injection lasers," *Opt. Eng.*, vol. 41, no. 12, pp. 3193–3203, Dec. 2002, doi: [10.1117/1.1518677](https://doi.org/10.1117/1.1518677).
- [14] D. Bimberg et al., "High-power high-brightness semiconductor lasers based on novel waveguide concepts," in *Proc. Novel -Plane Semicond. Lasers IX*, Feb. 2010, vol. 7616, pp. 321–334, doi: [10.1117/12.846577](https://doi.org/10.1117/12.846577).
- [15] I. I. Novikov et al., "High-power single mode (>1W) continuous wave operation of longitudinal photonic band crystal lasers with a narrow vertical beam divergence," *Appl. Phys. Lett.*, vol. 92, no. 10, Mar. 2008, Art. no. 103515, doi: [10.1063/1.2898517](https://doi.org/10.1063/1.2898517).
- [16] Z. Chen et al., "High power and narrow vertical divergence laser diodes with photonic crystal structure," *IEEE Photon. Technol. Lett.*, vol. 33, no. 8, pp. 399–402, Apr. 2021, doi: [10.1109/LPT.2021.3065963](https://doi.org/10.1109/LPT.2021.3065963).
- [17] M. V. Maximov et al., "High-performance 640-nm-range GaInP-AlGaInP lasers based on the longitudinal photonic bandgap crystal with narrow vertical beam divergence," *IEEE J. Quantum Electron.*, vol. 41, no. 11, pp. 1341–1348, Nov. 2005, doi: [10.1109/JQE.2005.857066](https://doi.org/10.1109/JQE.2005.857066).
- [18] T. Kaul, G. Erbert, A. Klehr, A. Maasdorf, D. Martin, and P. Crump, "Impact of carrier nonpinning effect on thermal power saturation in GaAs-based high power diode lasers," *IEEE J. Sel. Top. Quantum Electron.*, vol. 25, no. 6, Nov. 2019, Art. no. 1501910, doi: [10.1109/JSTQE.2019.2922109](https://doi.org/10.1109/JSTQE.2019.2922109).
- [19] D. M. Byrne and B. A. Keating, "A laser diode model based on temperature dependent rate equations," *IEEE Photon. Technol. Lett.*, vol. 1, no. 11, pp. 356–359, Nov. 1989, doi: [10.1109/68.43375](https://doi.org/10.1109/68.43375).
- [20] K. H. Hasler et al., "Comparative theoretical and experimental studies of two designs of high-power diode lasers," *Semicond. Sci. Technol.*, vol. 29, no. 4, Apr. 2014, Art. no. 045010, doi: [10.1088/0268-1242/29/4/045010](https://doi.org/10.1088/0268-1242/29/4/045010).
- [21] B. Li et al., "Analysis on high temperature characteristic of high power semiconductor laser array," *Chin. J. Lumin.*, vol. 41, no. 9, pp. 1158–1164, 2020, doi: [10.37188/fgxb20204109.1158](https://doi.org/10.37188/fgxb20204109.1158).
- [22] L. Wang, H. Qu, A. Qi, X. Zhou, and W. Zheng, "High-power laser diode at 9xx nm with 81.10% efficiency," *Opt. Lett.*, vol. 47, no. 13, pp. 3231–3234, Jul. 2022, doi: [10.1364/OL.452048](https://doi.org/10.1364/OL.452048).